Journal of
Applied and Computational Mechanics

Shahid Chamran
University of Ahvaz

Research Article

Differential Quadrature Method for Dynamic Buckling of Graphene Sheet Coupled by a Viscoelastic Medium Using Neperian Frequency Based on Nonlocal Elasticity Theory

Mohammad Malikan, Mohammad N. Sadraee Far

Department of Mechanical Engineering, Islamic Azad University, Mashhad, Iran

Abstract. In the present study, the dynamic buckling of the graphene sheet coupled by a viscoelastic matrix was studied. In light of the simplicity of Eringen's non-local continuum theory to considering the nanoscale influences, this theory was employed. Equations of motion and boundary conditions were obtained using Mindlin plate theory by taking nonlinear strains of von Kármán and Hamilton's principle into account. On the other hand, a viscoelastic matrix was modeled as a three-parameter foundation. Furthermore, the differential quadrature method was applied by which the critical load was obtained. Finally, since there was no research available for the dynamic buckling of a nanoplate, the static buckling was taken into consideration to compare the results and explain some significant and novel findings. One of these results showed that for greater values of the nanoscale parameter, the small scale had further influences on the dynamic buckling.

Keywords: Dynamic buckling; Graphene sheet; Viscoelastic matrix; Differential Quadrature method

1. Introduction

The study of dynamic stability of structures under impact loads was conducted over the past two decades. The main concept of the dynamic buckling is the stability of structures under time-dependent loads. The dynamic problems based on the type of load and the structural behavior are divided into three categories: high-velocity, mean-velocity, and low-velocity impact buckling. In the event that the loading time is very low (high velocity), within a few microseconds, and regarding high values of the load, the loading can be simplified as a pulse load called the pulse buckling. In problems with an applied load under the low velocity, the load value is lower and the loading time is much more than other problems. This type of loading can be simulated as a step load with a limited value and a high applied duration [1].

Mechanical analysis of nanostructural elements, in particular the nano-graphene sheet, under an in-plane impact load is an interesting problem. In fact, if a plate is loaded suddenly and then the load is released, the plate can sustain a much higher load than the static load. Most researchers have worked on the static buckling of nanoplates and far less (given the authors' awareness) on the dynamic in-plane resistance. Concerning the dynamic buckling studies of nano-graphene sheets, Hosseini-Ara et al. [2] have studied the buckling of a nanotube under thermal effects based on the non-local theory and applied classical continuum theory to derive the linear equations. Haftchenari et al. [3] have studied the dynamic analysis of a composite shell using a numerical method. The formulation was based on the Love's thin shell theory. Tamura and Babcock [4] have investigated the buckling of a cylindrical shell under a dynamic load. The critical step load required to produce the buckling of a cylindrical shell was determined by an approximate method and taking into account the inertia in the axial direction. Jabareen and Sheinman [5] have presented the buckling of beams on a foundation with the nonlinear elastic behavior under a rectangular

dynamic load. They used the classical plate theory to derive equations and an analytical method was used to solve governing equations. The nonlinear dynamic buckling of imperfect rectangular plates with different boundary conditions subjected to various pulse functions and using the Galerkin method was presented by Ramezannezhad Azarboni et al. [6]. They used the classical plate theory and nonlinear strains. Wang et al. [7] have investigated the dynamic stability of multi-walled carbon nanotube-reinforced composites via an analytical method. They used Donnell-shell theory and considered surface effects of nanomaterials. Petry and Fahlbusch [8] have studied the buckling of a plate exposed to dynamic loads using the simply supported boundary condition via the classical plate theory. Kubiak [9] have proposed the criteria of dynamic buckling estimation of a thin structure exposed to pulse loads.

In the present research, the dynamic stability of the orthotropic graphene sheet (Gs) is investigated. For this purpose, the plate is embedded in a viscoelastic matrix and governing equations are derived with the help of the first order shear deformation theory based on the von Kármán residual strains and with respect to the non-local continuum theory of Eringen. The equations in conjunction with boundary conditions are solved by the differential quadrature method (DQM). All in all, the outcomes of buckling force are investigated by changing many measurable factors, for example; the nanoscale parameter, dimensions of the plate, the growing ratio and the viscoelastic medium.

2. Mathematical formulation

The Gs is modeled as a rectangular nanoplate and the foundation is defined by a three-parameter viscoelastic foundation. An elastic foundation is the one in which both in-plane and pressure resistances are exhibited as a shear parameter and stiffness modulus. As a matter of fact, a polymer material could be defined as an elastic matrix in static analyses. On the other hand, in order to examine the dynamic analysis, for both plate and foundation, the viscoelasticity property can be taken into consideration (in the present paper, the viscoelastic property for the graphene sheet is neglected). In fact, the property is used for strengthening the materials against impact loads by which they can show flexibility. Generally speaking, viscoelasticity is a property of materials that show both viscous and elastic characteristics. Some polymers as well as metals display viscoelastic effects at high temperatures.

Fig. 1 shows the idealized and continuum paradigm for a Gs resting on the three-parameter foundation with length L_x, width L_y, and thickness h collateral to the $x, y,$ and z axes of the right-handed coordinate system, respectively.
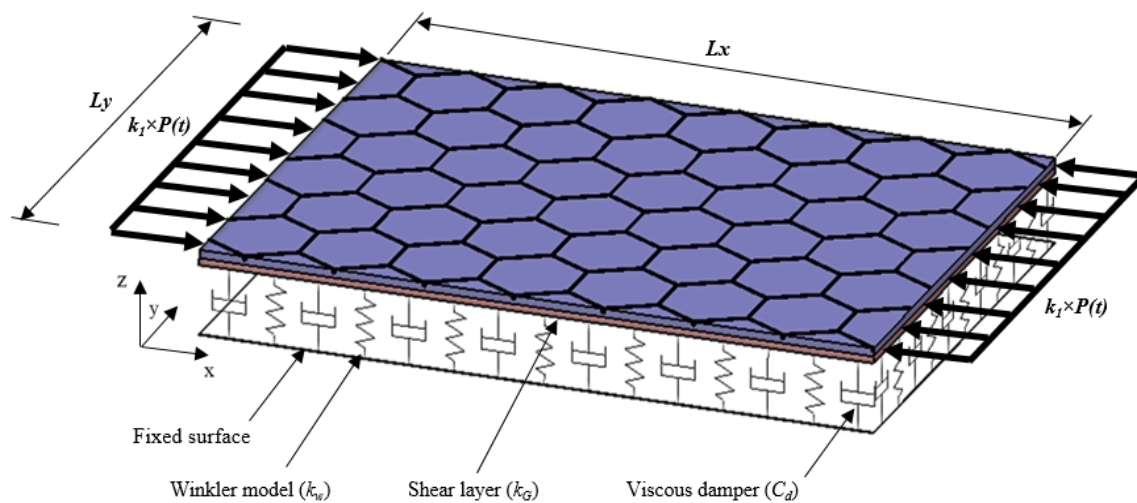

Fig. 1. Schematic appearance of the graphene sheet on the viscoelastic foundation

Based on the first order shear deformation theory and by using Hamilton's principle, the governing equations are formulated. Regarding the theory, the displacement field is developed as follows:

$$U\left(x, y, z, t\right) = u\left(x, y, t\right) + z\varphi\left(x, y, t\right) \tag{1a}$$

$$V\left(x, y, z, t\right) = v\left(x, y, t\right) + z\psi\left(x, y, t\right) \tag{1b}$$

$$W\left(x, y, z, t\right) = w\left(x, y, t\right) \tag{1c}$$

In Eqs. (1), the movement components of the neutral axis at $x, y,$ and z directions are $u, v,$ and w, respectively. For defining the swirl of plate elements around y and x axis, φ and ψ are used. The orthotropic nanoplate is considered for which properties is defined as follows:

$$[C] = \begin{bmatrix} \dfrac{E_x}{1-\nu_{xy}\nu_{yx}} & \dfrac{\nu_{xy}E_y}{1-\nu_{xy}\nu_{yx}} & 0 & 0 & 0 \\[2mm] \dfrac{\nu_{yx}E_x}{1-\nu_{xy}\nu_{yx}} & \dfrac{E_y}{1-\nu_{xy}\nu_{yx}} & 0 & 0 & 0 \\[2mm] 0 & 0 & G_{yz} & 0 & 0 \\[1mm] 0 & 0 & 0 & G_{xz} & 0 \\[1mm] 0 & 0 & 0 & 0 & G_{xy} \end{bmatrix} \tag{2}$$

Considering the von Kármán hypothesis, the Lagrangian strains are exhibited as [10]:

$$\varepsilon_{xx} = \frac{\partial u}{\partial x} + z\frac{\partial \varphi}{\partial x} + \frac{1}{2}\left(\frac{\partial w}{\partial x}\right)^2, \quad \varepsilon_{yy} = \frac{\partial v}{\partial y} + z\frac{\partial \psi}{\partial y} + \frac{1}{2}\left(\frac{\partial w}{\partial y}\right)^2, \quad \gamma_{xz} = \frac{\partial w}{\partial x} + \varphi, \quad \gamma_{yz} = \frac{\partial w}{\partial y} + \psi$$

$$\gamma_{xy} = \left(\frac{\partial u}{\partial y} + \frac{\partial v}{\partial x}\right) + z\left(\frac{\partial \varphi}{\partial y} + \frac{\partial \psi}{\partial x}\right) + \frac{\partial w}{\partial x}\frac{\partial w}{\partial y} \tag{3a-e}$$

For defining the potential energy in the whole domain of the plate, the following equation is available:

$$\Lambda = \int_0^t (\delta S - \delta T + \delta V)dt = 0 \tag{4}$$

where S is the energy stemmed from strains, T is the energy raised from movements, and also V is a work which are done upon an external object as a force. The strain energy by kronecker delta is expanded as follows:

$$\delta S = \iiint_v \left(\sigma_{xx}\delta\varepsilon_{xx} + \sigma_{yy}\delta\varepsilon_{yy} + \sigma_{xy}\delta\varepsilon_{xy} + \sigma_{xz}\delta\varepsilon_{xz} + \sigma_{yz}\delta\varepsilon_{yz}\right)dV = 0 \tag{5}$$

The kinetic energy of the orthotropic plate via FSDT is calculated as

$$T = \frac{1}{2}\int_{-h/2}^{h/2}\int_A \rho(z,T)\left(\left(\frac{\partial U}{\partial t}\right)^2 + \left(\frac{\partial V}{\partial t}\right)^2 + \left(\frac{\partial W}{\partial t}\right)^2\right)dAdz = 0 \tag{6}$$

Therefore, the kinetic energy in the figurative form is expanded as

$$\delta T = \int_{-h/2}^{h/2}\int_A \left[I_0\left(\frac{\partial u}{\partial t}\frac{\partial\delta u}{\partial t} + \frac{\partial v}{\partial t}\frac{\partial\delta v}{\partial t} + \frac{\partial w}{\partial t}\frac{\partial\delta w}{\partial t}\right) + I_1\left(\frac{\partial\varphi}{\partial t}\frac{\partial\delta u}{\partial t} + \frac{\partial u}{\partial t}\frac{\partial\delta\varphi}{\partial t} + \frac{\partial\psi}{\partial t}\frac{\partial\delta v}{\partial t} + \frac{\partial v}{\partial t}\frac{\partial\delta\psi}{\partial t}\right) + \right.$$
$$\left. I_2\left(\frac{\partial\varphi}{\partial t}\frac{\partial\delta\varphi}{\partial t} + \frac{\partial\psi}{\partial t}\frac{\partial\delta\psi}{\partial t}\right)\right]dAdz = 0 \tag{7}$$

in which the mass moments of inertias are presented as follows:

$$(I_0, I_1, I_2) = \int_A \rho(z,T)(1, z, z^2)dA \tag{8}$$

When the mechanical behavior of nanoplates and generally thin plates are studied, the plates should be deployed on a base as an impressive stability factor. In this paper, an elastic foundation called Pasternak is used and due to examining a dynamic problem, a viscous matrix is added to Pasternak medium in order to consider the damper effects in the foundation. Indeed, the effect of damping is needed to consider in the foundation while the plate is under dynamic loads. For this aim, the Visco-Pasternak foundation is developed as an external force defined as follows [11]:

$$V = \int_0^{L_y}\int_0^{L_x}\left(k_G\nabla^2 w - k_w w - C_d\frac{\partial w}{\partial t}\right)\delta w\, dx dy \tag{9}$$

Where k_w, k_G, and C_d denote Winkler, Pasternak, and Damper modulus parameters, respectively. By applying the variational formulation, the nonlinear equations of motion are derived as

$$\frac{\partial N_x^{NL}}{\partial x} + \frac{\partial N_{xy}^{NL}}{\partial y} - I_0\frac{\partial^2 u}{\partial t^2} - I_1\frac{\partial^2\varphi}{\partial t^2} = 0 \tag{10a}$$

$$\frac{\partial N_y^{NL}}{\partial y} + \frac{\partial N_{xy}^{NL}}{\partial x} - I_0\frac{\partial^2 v}{\partial t^2} - I_1\frac{\partial^2\psi}{\partial t^2} = 0 \tag{10b}$$

$$\frac{\partial Q_x^{NL}}{\partial x} + \frac{\partial Q_y^{NL}}{\partial y} + N_x^{NL}\frac{\partial^2 w}{\partial x^2} + 2N_{xy}^{NL}\frac{\partial^2 w}{\partial x\partial y} + N_y^{NL}\frac{\partial^2 w}{\partial y^2} + k_G\nabla^2 w - k_w w - C_d\frac{\partial w}{\partial t} - I_0\frac{\partial^2 w}{\partial t^2} = 0 \tag{10c}$$

$$\frac{\partial M_x^{NL}}{\partial x} + \frac{\partial M_{xy}^{NL}}{\partial y} - Q_x^{NL} - \left(I_1\frac{\partial^2 u}{\partial t^2} + I_2\frac{\partial^2\varphi}{\partial t^2}\right) = 0 \tag{10d}$$

$$\frac{\partial M_{xy}^{NL}}{\partial x} + \frac{\partial M_{y}^{NL}}{\partial y} - Q_{y}^{NL} - \left(I_1 \frac{\partial^2 v}{\partial t^2} + I_2 \frac{\partial^2 \psi}{\partial t^2} \right) = 0 \tag{10e}$$

where the non-local stress resultants are shown by index *NL,* and thereafter, index *L* denotes the local ones. The stress resultants in the local form are specified by the following relations:

$$\left(N_x^L, N_y^L, N_{xy}^L \right) = \int_{-\frac{h}{2}}^{\frac{h}{2}} \left(\sigma_x, \sigma_y, \sigma_{xy} \right) dz \tag{11a}$$

$$\left(M_x^L, M_y^L, M_{xy}^L \right) = \int_{-\frac{h}{2}}^{\frac{h}{2}} \left(\sigma_x, \sigma_y, \sigma_{xy} \right) z dz \tag{11b}$$

$$\left(Q_x^L, Q_y^L \right) = k_s \times \int_{-\frac{h}{2}}^{\frac{h}{2}} \left(\sigma_{xz}, \sigma_{yz} \right) dz \tag{11c}$$

In Eqs. (11c), k_s is a factor for correcting the shear stress distribution over the thickness in the FSDT plate. Regarding a non-local continuum principle created by Eringen, the nanoscale influences and forces generated by atoms are embedded into constitutive equations directly [12]. The nonlocal stress tensor is as follows:

$$\sigma_j^{NL}(X) = \int_v k\left(|X' - X|, \tau \right) [C] \varepsilon_j(X') dX' \tag{12}$$

A differential form of Eq. (12) is as follows [12]:

$$\left(1 - \mu \nabla^2 \right) \sigma_j^{NL} = \sigma_j^L \ , \ j = x, y, xy, \ \mu = (e_0 a)^2 \tag{13}$$

in which $e_0 a$ term is equal to $(0 < e_0 a \leq 2nm)$ [13-15]. Moreover, ∇^2 is the Laplace operator as follows:

$$\nabla^2 = \frac{\partial^2}{\partial x^2} + \frac{\partial^2}{\partial y^2} \tag{14}$$

Afterwards, the stress resultants are related to each other in both local and non-local subjects with the help of Eq. (13):

$$\left(1 - \mu \nabla^2 \right) N_j^{NL} = N_j^L, j = x, y, xy, \ \left(1 - \mu \nabla^2 \right) M_j^{NL} = M_j^L, j = x, y, xy, \ \left(1 - \mu \nabla^2 \right) Q_j^{NL} = Q_j^L, j = x, y \tag{15a-c}$$

Subsequently, by substituting Eqs. (15) into Eqs. (10), the nonlinear equations of motion can be rewritten as

$$\frac{\partial N_x^L}{\partial x} + \frac{\partial N_{xy}^L}{\partial y} - I_0 \left(\frac{\partial^2 u}{\partial t^2} - \mu \nabla^2 \frac{\partial^2 u}{\partial t^2} \right) - I_1 \left(\frac{\partial^2 \varphi}{\partial t^2} - \mu \nabla^2 \frac{\partial^2 \varphi}{\partial t^2} \right) = 0 \tag{16a}$$

$$\frac{\partial N_y^L}{\partial y} + \frac{\partial N_{xy}^L}{\partial x} - I_0 \left(\frac{\partial^2 v}{\partial t^2} - \mu \nabla^2 \frac{\partial^2 v}{\partial t^2} \right) - I_1 \left(\frac{\partial^2 \psi}{\partial t^2} - \mu \nabla^2 \frac{\partial^2 \psi}{\partial t^2} \right) = 0 \tag{16b}$$

$$\frac{\partial Q_x^L}{\partial x} + \frac{\partial Q_y^L}{\partial y} + N_x^L \frac{\partial^2 w}{\partial x^2} + 2 N_{xy}^L \frac{\partial^2 w}{\partial x \partial y} + N_y^L \frac{\partial^2 w}{\partial y^2} + k_G \nabla^2 w - k_w w - C_d \frac{\partial w}{\partial t} - \mu \nabla^2 \times$$
$$\left(N_x^L \frac{\partial^2 w}{\partial x^2} + 2 N_{xy}^L \frac{\partial^2 w}{\partial x \partial y} + N_y^L \frac{\partial^2 w}{\partial y^2} + k_G \nabla^2 w - k_w w - C_d \frac{\partial w}{\partial t} \right) - I_0 \left(\frac{\partial^2 w}{\partial t^2} - \mu \nabla^2 \frac{\partial^2 w}{\partial t^2} \right) = 0 \tag{16c}$$

$$\frac{\partial M_x^L}{\partial x} + \frac{\partial M_{xy}^L}{\partial y} - Q_x^L - I_1 \left(\frac{\partial^2 u}{\partial t^2} - \mu \nabla^2 \frac{\partial^2 u}{\partial t^2} \right) - I_2 \left(\frac{\partial^2 \varphi}{\partial t^2} - \mu \nabla^2 \frac{\partial^2 \varphi}{\partial t^2} \right) = 0 \tag{16d}$$

$$\frac{\partial M_{xy}^L}{\partial x} + \frac{\partial M_y^L}{\partial y} - Q_x^L - I_1 \left(\frac{\partial^2 v}{\partial t^2} - \mu \nabla^2 \frac{\partial^2 v}{\partial t^2} \right) - I_2 \left(\frac{\partial^2 \psi}{\partial t^2} - \mu \nabla^2 \frac{\partial^2 \psi}{\partial t^2} \right) = 0 \tag{16e}$$

Moreover, all boundary conditions are satisfied by the following equation originated from the energy variational formulation. These boundary conditions are used in the solution section.

$$\delta S_{boundaries} = \int \left[N_y \delta v + N_{xy} \delta u + M_{xy} \delta \varphi + M_y \delta \psi + \left(Q_y + N_y \frac{\partial w}{\partial y} + N_{xy} \frac{\partial w}{\partial x} \right) \delta w \right] dx$$
$$+ \int \left[N_x \delta u + N_{xy} \delta v + M_x \delta \varphi + M_{xy} \delta \psi + \left(Q_x + N_x \frac{\partial w}{\partial x} + N_{xy} \frac{\partial w}{\partial y} \right) \delta w \right] dy \tag{17}$$

The equations obtained for the nanoplate under the in-plane step load are shown in Table 1 [6].

Table 1. Types of biaxial dynamic buckling loads

Load type	Function	Load type	Function
Sinusoidal	$N_r^s = \begin{cases} N_r \ \sin\left(\dfrac{\pi t}{lr}\right), 0 \leq t \leq T \\ 0, \ T < t \end{cases}$; r=x,y	Damping	$N_r^D = \begin{cases} N_r \ e^{-\left(\frac{\pi t}{lr}\right)} \sin\left(\dfrac{\pi t}{lr}\right), 0 \leq t \leq T \\ 0, \ T < t \end{cases}$; r=x,y
Exponential	$N_r^E = \begin{cases} N_r \ e^{-\left(\frac{\pi t}{lr}\right)}, 0 \leq t \leq T \\ 0, \ T < t \end{cases}$; r=x,y	Rectangular	$N_r^R = \begin{cases} N_r, 0 \leq t \leq T \\ 0, \ T < t \end{cases}$; r=x,y

By inserting the stress resultants in Eqs. (16), the nonlinear dynamic stability equations with respect to the displacement unknowns are provided as

$$-I_0\left(\frac{\partial^2 u}{\partial t^2} - \mu\nabla^2 \frac{\partial^2 u}{\partial t^2}\right) - I_1\left(\frac{\partial^2 \varphi}{\partial t^2} - \mu\nabla^2 \frac{\partial^2 \varphi}{\partial t^2}\right) = 0 \tag{18a}$$

$$-I_0\left(\frac{\partial^2 v}{\partial t^2} - \mu\nabla^2 \frac{\partial^2 v}{\partial t^2}\right) - I_1\left(\frac{\partial^2 \psi}{\partial t^2} - \mu\nabla^2 \frac{\partial^2 \psi}{\partial t^2}\right) = 0 \tag{18b}$$

$$H_{55}\left(\frac{\partial^2 w}{\partial x^2} + \frac{\partial \varphi}{\partial x}\right) + H_{44}\left(\frac{\partial^2 w}{\partial y^2} + \frac{\partial \psi}{\partial y}\right) - \mu\frac{\partial^4 w}{\partial x^2 \partial y^2}\left(N_x^R + N_y^R\right) + \left(N_x^R\right)\left(\frac{\partial^2 w}{\partial x^2} - \mu\frac{\partial^4 w}{\partial x^4}\right) +$$
$$\left(N_y^R\right)\left(\frac{\partial^2 w}{\partial y^2} - \mu\frac{\partial^4 w}{\partial y^4}\right) + \left(1 - \mu\nabla^2\right)\left(k_G\nabla^2 w - k_w w - C_d\frac{\partial w}{\partial t}\right) - I_0\left(\frac{\partial^2 w}{\partial t^2} - \mu\nabla^2 \frac{\partial^2 w}{\partial t^2}\right) = 0 \tag{18c}$$

$$D_{11}\frac{\partial^2 \varphi}{\partial x^2} + \left(D_{12} + D_{66}\right)\frac{\partial^2 \psi}{\partial x \partial y} + D_{66}\frac{\partial^2 \varphi}{\partial y^2} - H_{55}\left(\frac{\partial w}{\partial x} + \varphi\right) - I_1\left(\frac{\partial^2 u}{\partial t^2} - \mu\nabla^2 \frac{\partial^2 u}{\partial t^2}\right) - I_2\left(\frac{\partial^2 \varphi}{\partial t^2} - \mu\nabla^2 \frac{\partial^2 \varphi}{\partial t^2}\right) = 0 \tag{18d}$$

$$D_{22}\frac{\partial^2 \psi}{\partial y^2} + \left(D_{12} + D_{66}\right)\frac{\partial^2 \varphi}{\partial x \partial y} + D_{66}\frac{\partial^2 \psi}{\partial x^2} - H_{44}\left(\frac{\partial w}{\partial y} + \psi\right) - I_1\left(\frac{\partial^2 v}{\partial t^2} - \mu\nabla^2 \frac{\partial^2 v}{\partial t^2}\right) - I_2\left(\frac{\partial^2 \psi}{\partial t^2} - \mu\nabla^2 \frac{\partial^2 \psi}{\partial t^2}\right) = 0 \tag{18e}$$

in which N_x^R, N_y^R are the in-plane step loads in the biaxial dynamic buckling. In order to study the dynamic stability of the graphene sheet, a solution for the displacement and rotation fields ($k\ (x,y,t)$) is assumed and exerted in the following form [2, 16-17]:

$$k(x,y,t) = k_1(x,y) \times e^{ft}, \ (k = u, v, w, \varphi, \psi; \ k_1 = u_1, v_1, w_1, \varphi_1, \psi_1) \tag{19}$$

where $k\ (x,y,t)$ are time independent parameters and $k_1\ (x,y)$ are the magnitude of $k\ (x,y,t)$. Moreover, f is the complex frequency that is a type of frequency dependent on two parameters and is presented as $f = \sigma + \theta\omega\ (\theta = \sqrt{-1})$. The real term of f is defined as the neper frequency ($\sigma\ (Neper/s)$) which controls magnitude of a signal and shows a growing ratio with respect to instability. Furthermore, the imaginary term is called ω which controls rotation of a signal and also demonstrates the rotational speed or angular frequency (Rad/s) of a vibrational mechanism [2, 16-17].

By substituting Eq. (19) into Eqs. (18), Eqs. (18) are rewritten as follows:

$$-I_0\sigma^2\left(u_1 - \mu\left(\frac{\partial^2 u_1}{\partial x^2} + \frac{\partial^2 u_1}{\partial y^2}\right)\right) - I_1\sigma^2\left(\varphi_1 - \mu\left(\frac{\partial^2 \varphi_1}{\partial x^2} + \frac{\partial^2 \varphi_1}{\partial y^2}\right)\right) = 0 \tag{20a}$$

$$-I_0\sigma^2\left(v_1 - \mu\left(\frac{\partial^2 v_1}{\partial x^2} + \frac{\partial^2 v_1}{\partial y^2}\right)\right) - I_1\sigma^2\left(\psi_1 - \mu\left(\frac{\partial^2 \psi_1}{\partial x^2} + \frac{\partial^2 \psi_1}{\partial y^2}\right)\right) = 0 \tag{20b}$$

$$H_{55}\left(\frac{\partial^2 w_1}{\partial x^2} + \frac{\partial \varphi_1}{\partial x}\right) + H_{44}\left(\frac{\partial^2 w_1}{\partial y^2} + \frac{\partial \psi_1}{\partial y}\right) - \mu\frac{\partial^4 w_1}{\partial x^2 \partial y^2}\left(N_x^R + N_y^R\right) + \left(N_x^R\right)\left(\frac{\partial^2 w_1}{\partial x^2} - \mu\frac{\partial^4 w_1}{\partial x^4}\right) +$$
$$\left(N_y^R\right)\left(\frac{\partial^2 w_1}{\partial y^2} - \mu\frac{\partial^4 w_1}{\partial y^4}\right) + \left(1 - \mu\left(\frac{\partial^2}{\partial x^2} + \frac{\partial^2}{\partial y^2}\right)\right) \times \left(k_G\left(\frac{\partial^2 w_1}{\partial x^2} + \frac{\partial^2 w_1}{\partial y^2}\right) - k_w w_1 - \sigma C_d w_1\right) -$$
$$I_0\sigma^2\left(w_1 - \mu\left(\frac{\partial^2 w_1}{\partial x^2} + \frac{\partial^2 w_1}{\partial y^2}\right)\right) = 0 \tag{20c}$$

$$D_{11}\frac{\partial^2\varphi_1}{\partial x^2}+\left(D_{12}+D_{66}\right)\frac{\partial^2\psi_1}{\partial x\partial y}+D_{66}\frac{\partial^2\varphi_1}{\partial y^2}-H_{55}\left(\frac{\partial w_1}{\partial x}+\varphi_1\right)-I_1\sigma^2\left(u_1-\mu\left(\frac{\partial^2 u_1}{\partial x^2}+\frac{\partial^2 u_1}{\partial y^2}\right)\right)-$$

$$I_2\sigma^2\left(\varphi_1-\mu\left(\frac{\partial^2\varphi_1}{\partial x^2}+\frac{\partial^2\varphi_1}{\partial y^2}\right)\right)=0 \tag{20d}$$

$$D_{22}\frac{\partial^2\psi_1}{\partial y^2}+\left(D_{12}+D_{66}\right)\frac{\partial^2\varphi_1}{\partial x\partial y}+D_{66}\frac{\partial^2\psi_1}{\partial x^2}-H_{44}\left(\frac{\partial w_1}{\partial y}+\psi_1\right)-I_1\sigma^2\left(v_1-\mu\left(\frac{\partial^2 v_1}{\partial x^2}+\frac{\partial^2 v_1}{\partial y^2}\right)\right)-$$

$$I_2\sigma^2\left(\psi_1-\mu\left(\frac{\partial^2\psi_1}{\partial x^2}+\frac{\partial^2\psi_1}{\partial y^2}\right)\right)=0 \tag{20e}$$

For convenience, the equations are rewritten in terms of non-dimensional variables produced as follows:

$$W_1=\frac{w_1}{L_x},\ \alpha=\frac{L_x}{h},\ \Phi_1=\varphi_1,\ \Psi_1=\psi_1,\ \eta=\frac{x}{L_x},\ \xi=\frac{y}{L_y},\ \beta=\frac{L_x}{L_y},K_G=\frac{k_G}{G_{xy}\times h},$$

$$K_W=\frac{k_w\times L_x^2}{G_{xy}\times h},\ \Omega=\sigma L_x\sqrt{\frac{\rho}{G_{xy}}},\ U_1=\frac{u_1}{L_x},\ V_1=\frac{v_1}{L_x},\ \lambda_1=\frac{H_{55}\times L_x^2}{G_{xy}\times h^3},\ \lambda_2=\frac{H_{44}\times L_x^2}{G_{xy}\times h^3},$$

$$C_D=\frac{C_d}{\sqrt{G_{xy}I_0}},\ \varepsilon=\frac{L_x}{\sqrt{h}},\ \tau_0=\frac{I_0}{I_0},\ \tau_1=\frac{I_1}{I_0 h},\ \tau_2=\frac{I_2}{I_0 h^2},\ \delta_1=\frac{D_{11}}{G_{xy}\times h^3},\ \delta_2=\frac{D_{22}}{G_{xy}\times h^3}, \tag{21}$$

$$\delta_3=\frac{D_{12}}{G_{xy}\times h^3},\ \delta_4=\frac{D_{66}}{G_{xy}\times h^3},\ \Gamma=\frac{\mu}{L_x^2}$$

Subsequently, Eqs. (20) are obtained as follows:

$$-\Omega^2\left(U_1-\Gamma\left(\frac{\partial^2 U_1}{\partial\eta^2}+\beta^2\frac{\partial^2 U_1}{\partial\xi^2}\right)\right)-\left(\frac{\Omega^2}{\alpha}\right)\left(\Phi_1-\Gamma\left(\frac{\partial^2\Phi_1}{\partial\eta^2}+\beta^2\frac{\partial^2\Phi_1}{\partial\xi^2}\right)\right)=0 \tag{22a}$$

$$-\Omega^2\left(V_1-\Gamma\left(\frac{\partial^2 V_1}{\partial\eta^2}+\beta^2\frac{\partial^2 V_1}{\partial\xi^2}\right)\right)-\left(\frac{\Omega^2}{\alpha}\right)\left(\Psi_1-\Gamma\left(\frac{\partial^2\Psi_1}{\partial\eta^2}+\beta^2\frac{\partial^2\Psi_1}{\partial\xi^2}\right)\right)=0 \tag{22b}$$

$$\frac{\lambda_1}{\alpha^2}\left(\frac{\partial^2 W_1}{\partial\eta^2}+\frac{\partial\Phi_1}{\partial\eta}\right)+\frac{\lambda_2}{\alpha^2}\left(\beta^2\frac{\partial^2 W_1}{\partial\xi^2}+\beta\frac{\partial\Psi_1}{\partial\xi}\right)-\Gamma\beta^2\frac{\partial^4 W_1}{\partial\eta^2\partial\xi^2}\left(N_\eta+N_\xi\right)+N_\eta\left(\frac{\partial^2 W_1}{\partial\eta^2}-\Gamma\frac{\partial^4 W_1}{\partial\eta^4}\right)+$$

$$N_\xi\left(\beta^2\frac{\partial^2 W_1}{\partial\xi^2}-\Gamma\beta^4\frac{\partial^4 W_1}{\partial\xi^4}\right)-K_W\left(W_1-\Gamma\left(\frac{\partial^2 W_1}{\partial\eta^2}+\beta^2\frac{\partial^2 W_1}{\partial\xi^2}\right)\right)+K_G\left(1-\Gamma\left(\frac{\partial^2}{\partial\eta^2}+\beta^2\frac{\partial^2}{\partial\xi^2}\right)\right)\left(\frac{\partial^2 W_1}{\partial\eta^2}+\beta^2\frac{\partial^2 W_1}{\partial\xi^2}\right) \tag{22c}$$

$$-\left(\Omega C_D\varepsilon\right)\left(W_1-\Gamma\left(\frac{\partial^2 W_1}{\partial\eta^2}+\beta^2\frac{\partial^2 W_1}{\partial\xi^2}\right)\right)-\Omega^2\left(W_1-\Gamma\left(\frac{\partial^2 W_1}{\partial\eta^2}+\beta^2\frac{\partial^2 W_1}{\partial\xi^2}\right)\right)=0$$

$$\delta_1\frac{\partial^2\Phi_1}{\partial\eta^2}+\left(\delta_3+\delta_4\right)\beta\frac{\partial^2\Psi_1}{\partial\eta\partial\xi}+\delta_4\beta^2\frac{\partial^2\Phi_1}{\partial\xi^2}-\lambda_1\left(\frac{\partial W_1}{\partial\eta}+\Phi_1\right)-\left(\Omega^2\alpha\right)\left(U_1-\Gamma\left(\frac{\partial^2 U_1}{\partial\eta^2}+\beta^2\frac{\partial^2 U_1}{\partial\xi^2}\right)\right)-\Omega^2\times$$

$$\left(\Phi_1-\Gamma\left(\frac{\partial^2\Phi_1}{\partial\eta^2}+\beta^2\frac{\partial^2\Phi_1}{\partial\xi^2}\right)\right)=0 \tag{22d}$$

$$\delta_2\beta^2\frac{\partial^2\Psi_1}{\partial\xi^2}+\left(\delta_3+\delta_4\right)\beta\frac{\partial^2\Phi_1}{\partial\eta\partial\xi}+\delta_4\frac{\partial^2\Psi_1}{\partial\eta^2}-\lambda_2\left(\beta\frac{\partial W_1}{\partial\xi}+\Psi_1\right)-\left(\Omega^2\alpha\right)\left(V_1-\Gamma\left(\frac{\partial^2 V_1}{\partial\eta^2}+\beta^2\frac{\partial^2 V_1}{\partial\xi^2}\right)\right)-\Omega^2\times$$

$$\left(\Psi_1-\Gamma\left(\frac{\partial^2\Psi_1}{\partial\eta^2}+\beta^2\frac{\partial^2\Psi_1}{\partial\xi^2}\right)\right)=0 \tag{22e}$$

3. Differential quadrature method

The numerical methods to solve partial differential equations play a very important role in many engineering's sciences. Since the solutions of the equations are hard or impossible, they can be converted into simple and solvable equations by numerical methods. Although it is conjuncted with some minor errors, the results are acceptable. One of these numerical methods is the differential quadrature method (DQM) in which *nth* differential of continuous function *f (x, y)* based on the *x* at the point *x′* is written from weighting's functions at the whole points in a linear domain [18-19]. The method for the first time was proposed to solve the differential equations with initial values [20] and used for modelling several boundary conditions

[21]. Turning to the stability equations, DQM is now implemented in Eqs. (22) to discretize them [22-24]:

$$-\Omega^2\left(U_1 - \Gamma\left(\sum_{k=1}^{N} C_{ik}^{(2)} U_1(x_k, y_j) + \beta^2 \sum_{r=1}^{M} C_{jr}^{(2)} U_1(x_i, y_r)\right)\right) - \left(\frac{\Omega^2}{\alpha}\right)\left(\Phi_1 - \Gamma\left(\sum_{k=1}^{N} C_{ik}^{(2)} \Phi_1(x_k, y_j) + \beta^2 \sum_{r=1}^{M} C_{jr}^{(2)} \Phi_1(x_i, y_r)\right)\right) = 0$$

$$-\Omega^2\left(V_1 - \Gamma\left(\sum_{k=1}^{N} C_{ik}^{(2)} V_1(x_k, y_j) + \beta^2 \sum_{r=1}^{M} C_{jr}^{(2)} V_1(x_i, y_r)\right)\right) - \left(\frac{\Omega^2}{\alpha}\right)\left(\Psi_1 - \Gamma\left(\sum_{k=1}^{N} C_{ik}^{(2)} \Psi_1(x_k, y_j) + \beta^2 \sum_{r=1}^{M} C_{jr}^{(2)} \Psi_1(x_i, y_r)\right)\right) = 0$$

$$\frac{\lambda_1}{\alpha^2}\left(\sum_{k=1}^{N} C_{ik}^{(2)} W_1(x_k, y_j) + \sum_{k=1}^{N} C_{ik}^{(1)} \Phi_1(x_k, y_j)\right) + \frac{\lambda_2}{\alpha^2}\left(\beta^2 \sum_{r=1}^{M} C_{jr}^{(2)} W_1(x_i, y_r) + \beta \sum_{r=1}^{M} C_{jr}^{(1)} \Psi_1(x_i, y_r)\right)$$

$$-\Gamma\beta^2\left(N_\eta + N_\xi\right) \times \sum_{k=1}^{N}\sum_{r=1}^{M} C_{ik}^{(2)} W_1(x_k, y_r) C_{jr}^{(2)} + N_\eta \times \sum_{k=1}^{N} C_{ik}^{(2)} W_1(x_k, y_j) - \Gamma N_\eta \times \sum_{k=1}^{N} C_{ik}^{(4)} W_1(x_k, y_j)$$

$$+\beta^2 N_\xi \times \sum_{r=1}^{M} C_{jr}^{(2)} W_1(x_i, y_r) - \Gamma\beta^4 N_\xi \times \sum_{r=1}^{M} C_{jr}^{(4)} W_1(x_i, y_r) - K_W W_1 + K_W \Gamma \times$$

$$\left(\sum_{k=1}^{N} C_{ik}^{(2)} W_1(x_k, y_j) + \beta^2 \sum_{r=1}^{M} C_{jr}^{(2)} W_1(x_i, y_r)\right) + K_G\left(\sum_{k=1}^{N} C_{ik}^{(2)} W_1(x_k, y_j) + \beta^2 \sum_{r=1}^{M} C_{jr}^{(2)} W_1(x_i, y_r)\right)$$

$$-K_G\Gamma\left(\sum_{k=1}^{N} C_{ik}^{(4)} W_1(x_k, y_j) + 2\beta^2 \sum_{k=1}^{N}\sum_{r=1}^{M} C_{ik}^{(2)} W_1(x_k, y_r) C_{jr}^{(2)} + \beta^4 \sum_{r=1}^{M} C_{jr}^{(4)} W_1(x_i, y_r)\right)$$

$$-(\Omega C_D \varepsilon) \times \left(W_1 - \Gamma\left(\sum_{k=1}^{N} C_{ik}^{(2)} W_1(x_k, y_j) + \beta^2 \sum_{r=1}^{M} C_{jr}^{(2)} W_1(x_i, y_r)\right)\right) -$$

$$\Omega^2\left(W_1 - \Gamma\left(\sum_{k=1}^{N} C_{ik}^{(2)} W_1(x_k, y_j) + \beta^2 \sum_{r=1}^{M} C_{jr}^{(2)} W_1(x_i, y_r)\right)\right) = 0$$

$$\delta_1 \sum_{k=1}^{N} C_{ik}^{(2)} \Phi_1(x_k, y_j) + (\delta_3 + \delta_4)\beta \sum_{k=1}^{N}\sum_{r=1}^{M} C_{ik}^{(1)} \Psi_1(x_k, y_r) C_{jr}^{(1)} + \delta_4 \beta^2 \sum_{r=1}^{M} C_{jr}^{(2)} \Phi_1(x_i, y_r) - \lambda_1 \sum_{k=1}^{N} C_{ik}^{(1)} W_1(x_k, y_j) - \lambda_1 \Phi_1 -$$

$$\left(\Omega^2 \alpha\right)\left(U_1 - \Gamma\left(\sum_{k=1}^{N} C_{ik}^{(2)} U_1(x_k, y_j) + \beta^2 \sum_{r=1}^{M} C_{jr}^{(2)} U_1(x_i, y_r)\right)\right) - \Omega^2\left(\Phi_1 - \Gamma\left(\sum_{k=1}^{N} C_{ik}^{(2)} \Phi_1(x_k, y_j) + \beta^2 \sum_{r=1}^{M} C_{jr}^{(2)} \Phi_1(x_i, y_r)\right)\right) = 0$$

$$\delta_2 \beta^2 \sum_{k=1}^{M} C_{jr}^{(2)} \Psi_1(x_i, y_r) + \delta_4 \sum_{k=1}^{N} C_{ik}^{(2)} \Psi_1(x_k, y_j) + (\delta_3 + \delta_4)\beta \sum_{k=1}^{N}\sum_{r=1}^{M} C_{ik}^{(1)} \Phi_1(x_k, y_r) C_{jr}^{(1)} - \lambda_2 \beta \sum_{k=1}^{M} C_{jr}^{(1)} W_1(x_i, y_r) - \lambda_2 \Psi_1 -$$

$$\left(\Omega^2 \alpha\right)\left(V_1 - \Gamma\left(\sum_{k=1}^{N} C_{ik}^{(2)} V_1(x_k, y_j) + \beta^2 \sum_{r=1}^{M} C_{jr}^{(2)} V_1(x_i, y_r)\right)\right) - \Omega^2\left(\Psi_1 - \Gamma\left(\sum_{k=1}^{N} C_{ik}^{(2)} \Psi_1(x_k, y_j) + \beta^2 \sum_{r=1}^{M} C_{jr}^{(2)} \Psi_1(x_i, y_r)\right)\right) = 0$$

(23a-e)

By assembling Eqs. (23 a-e) with boundary conditions, an algebraic equation in the matrix form is obtained as follows [24]:

$$\begin{bmatrix} [K_{bb}] & [K_{bi}] \\ [K_{ib}] & [K_{ii}] \end{bmatrix}\begin{Bmatrix} d_b \\ d_i \end{Bmatrix} = N\begin{bmatrix} 0 & 0 \\ [KN_{ib}] & [KN_{ii}] \end{bmatrix}\begin{Bmatrix} d_b \\ d_i \end{Bmatrix}$$

(24)

in which $[K_{bb}]$ and $[K_{bi}]$ define submatrixes relating to boundary conditions, $[K_{ib}]$, $[K_{ii}]$, $[KN_{ib}]$, and $[KN_{ib}]$ denoting submatrixes related to stability equations. Furthermore, regarding displacements field, d_i and d_b explain inner and edge points, respectively. Subsequently, Eq. (24) is transformed into an eigenvalue equation by eliminating $\{d_b\}$ [24].

$$\left([K_{total}] - N[I]\right)\{d_i\} = 0$$

(25)

where $[K_{total}] = \left[[KN_{ib}][K_{bb}]^{-1}[K_{bi}] + [KN_{ii}]\right]^{-1}\left[-[K_{ib}][K_{bb}]^{-1}[K_{bi}] + [K_{ii}]\right]$ and I means a unit matrix. Therewith, by using a MATLAB program and using Eq. (25), the critical load (N) is obtained.

4. Boundary conditions

In the present study, to solve the equations, several kinds of boundaries are taken into account and applied in the standard form below:

Free edge (F):
$$Q_\eta = M_\eta = M_{\eta\xi} = 0 \;:\; \eta = 0,1$$
$$Q_\xi = M_\xi = M_{\eta\xi} = 0 \;:\; \xi = 0,1$$

(26)

Clamped (C):
$$W = \Psi = \Phi = 0 \quad : \quad \eta = 0,1$$
$$W = \Psi = \Phi = 0 \quad : \quad \xi = 0,1$$
(27)

Simply supported (S):
$$W = \Phi = M_\eta = 0 \quad : \quad \eta = 0,1$$
$$W = \Psi = M_\xi = 0 \quad : \quad \xi = 0,1$$
(28)

5. Results and discussions

To emphasize the numerical outcomes and due to the fact that there is not any research available to study the dynamic buckling of Gs, the static buckling is considered. Therefore, the results are compared with those of another study [22] as shown in Table 2. Besides, for further clarification, another research results [25] in which the molecular dynamic simulation was used is added to Table. 2. According to the validity section, the results are properly consistent with those of other studies.

Table 2. Comparison of results for critical biaxial static buckling loads of single-layered graphene sheet and all edges simply supported the results obtained from DQM [22], and molecular dynamics simulation [25], (Ref. [24] was added from a work related to the authors) *E=1TPa, υ=0.3, h=0.34nm, k_w=0, k_G=0, C_D=0, μ=1.81nm², β=1, k1=1, k2=1, SSSS*

Critical load (*Pa.m*)			Lx=Ly (nm)
Ref. [22]	MD results [25]	Ref. [24] σ=0 (Static buckling)	
1.0749	1.0837	1.0809	4.99
0.6523	0.6536	0.6519	8.080
0.4356	0.4331	0.4350	10.77
0.2645	0.2609	0.2639	14.65
0.1751	0.1714	0.1748	18.51
0.1239	0.1191	0.1237	22.35
0.0917	0.0889	0.0914	26.22
0.0707	0.0691	0.0705	30.04
0.0561	0.0554	0.0560	33.85
0.0453	0.0449	0.0451	37.81

Geometrical and mechanical properties of Gs and the foundation parameters used in the present study are taken from [26-31]. Moreover, the value of $\rho=2250\ kg/m^3$ is allocated for the density of graphene sheet [32]. First of all, the convergence rating for DQ method should be checked. For this purpose, grid points are changing on the basis of the two boundary conditions as shown in Fig. 2. As can be seen, in order to achieve precise and appropriate results, there is no need to use more than nine nodes for splitting the plate′s axis.
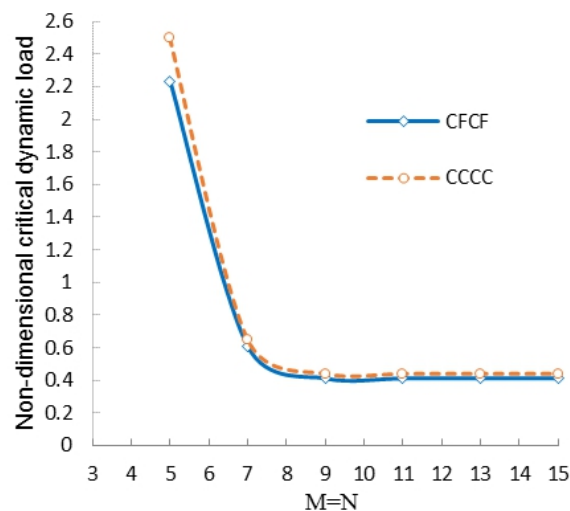

Fig. 2. Grid points convergence into two directions for the rectangular plate (*Ω=2, C_D=0.1, e₀a=2nm, k1=1; k2=0, Lx/Ly=1*).

The effects of nanoscale factor on the non-dimensional critical loads are presented in Figs. 3(a), (b), and (c). These figures illustrate that the non-local loads are smaller than local ones and much more differences are shown by an increase in σ parameter. It can also be mentioned that by an increase in the nanoscale factor, the critical loads decrease accordingly. This means that, the nanoscale factor has a reduction effect on buckling load values. In addition, the neper effects increase the critical buckling for a variety of nanoscale factors. As expected, the critical loads with σ=0 are lower than critical dynamic ones in the same conditions.
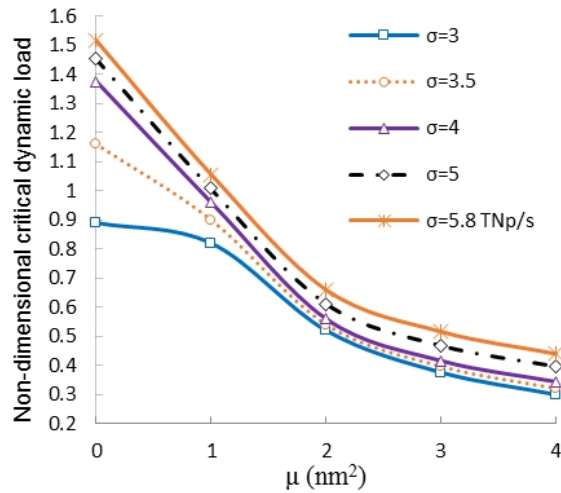
Fig. 3 (a). The influences of the nanoscale factor on the dimensionless critical dynamic load (*CCCC, C$_D$=0.1, k1=1; k2=0, β=1*)
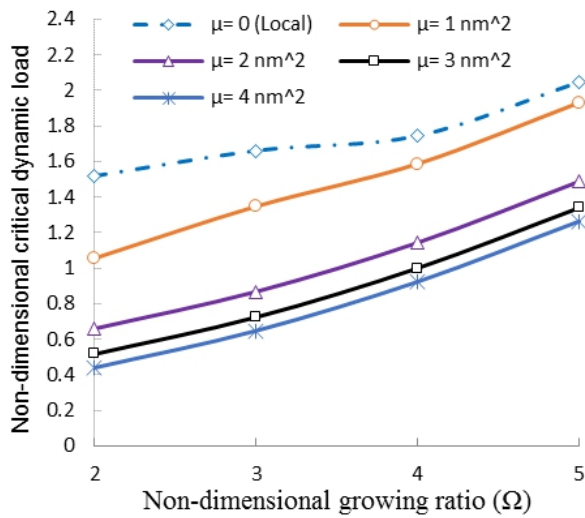

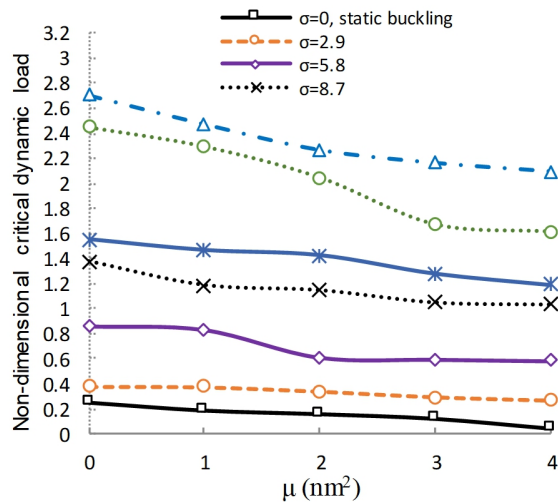**Fig. 3 (b).** Non-local parameter versus growing ratio (*CCCC, C$_D$=0.1, k1=1; k2=0, Lx/Ly=1*).

Fig. 3 (c). The influences of the nanoscale factor versus growing ratio (*CFCF, C$_D$=0.2, k1=0; k2=1, Lx/Ly=1*)

Fig. 4 indicates the influences of small scale factor on two kinds of loads. In the first and second cases, the dynamic load is into *x* (*k1=1, k2=0*) and *y* (*k1=0, k2=1*) directions, respectively. As shown, by having the critical load only into *y* direction, higher results are obtained in contrast to another one. It can be seen that by paying attention to *e$_0$a=0*, the gap of the results is becoming less than other studies. Although, by considering and increasing the nanoscale factor, the difference will be greater. Therefore, it can be concluded that the increase of small scale parameter is more effective than the orthotropic plate influences for both cases of load direction.
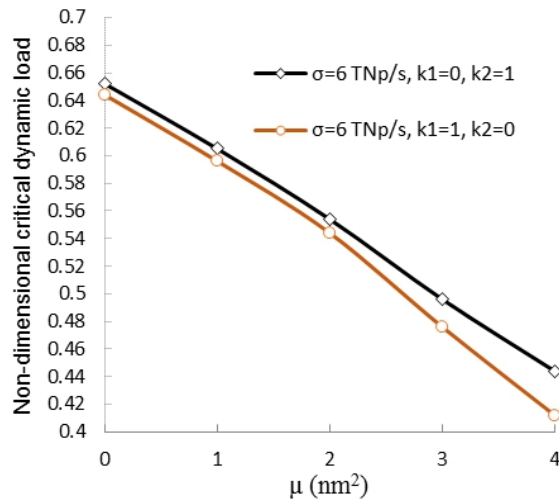
Fig. 4. Comparing *x*, *y* axial critical dynamic load**s** (*CFCF*, C_D=0.1, *Lx/Ly=1*).

Fig. 5 is plotted based on the several boundary conditions versus the nanoscale parameter to reveal the critical dynamic load. It is illustrated that if the numbers of free edges increase, the impact of the nanoscale factor on borderline conditions will decrease. Besides, regarding less flexible borders, the dynamic loads will be raised. As can be seen, for whole constraints between μ=0 and μ=2nm^2, the lines have a steep slope and a downward trend. Although, for values of more than μ=2nm^2, the slope of the diagrams may be approximately gradual. Moreover, by the increase of the nanoscale factor, the dynamic loads for different boundaries are nearly close to each other.
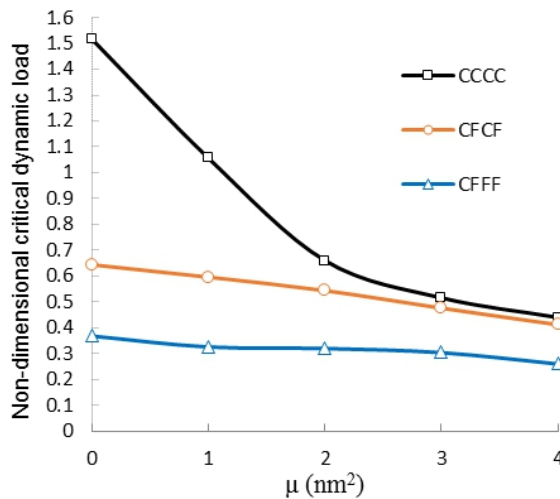
Fig. 5. The effects of small scale parameter on various boundary conditions (*Ω=2*, C_D=0.1, *k1=1; k2=0, Lx/Ly=1*)
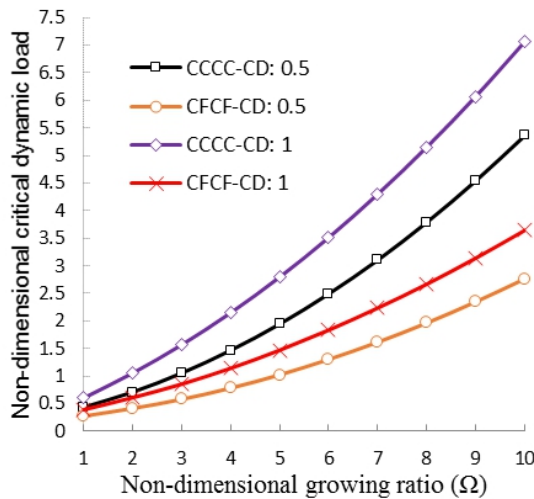
Fig. 6. Growing ratio versus different types of boundary conditions (*e₀a=2nm, k1=1; k2=0, β=1*).

Fig. 6 presents the influences of growing ratio versus the viscous parameter for the non-local critical dynamic load. It can be seen that by an increase in the growing ratio, the difference of results for two boundary conditions will increase as well. It is obvious that as the flexibility of boundary conditions decrease, the difference between outcomes in two damper's values will decrease as well. Fig. 7 illustrates the critical dimensionless load versus Winkler stiffness of viscoelastic medium in various boundary conditions. It can be seen that by taking less flexible boundaries into consideration, the changes in k_w have more impact on the dynamic loads. In addition, after adding certain value of the medium's stiffness, the increase of the Winkler parameter will not be comprehensible.

Fig. 8 shows the effect of the viscous parameter in various boundary conditions. The effects of viscous damper in CCCC will be higher than the other ones. Moreover, it is obvious that by increasing the damping value, the differences among various boundary conditions will increase as well.
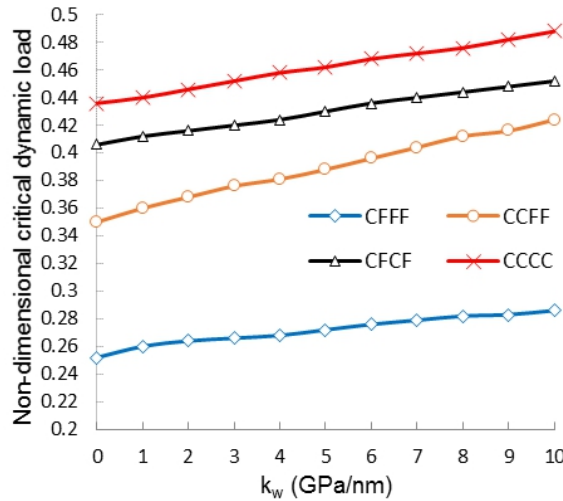

Fig. 7. Winkler stiffness in viscoelastic foundation versus various boundary conditions ($\Omega=2$, $C_D=0.1$, $e_0a=2nm$, $k1=1$; $k2=0$, $\beta=1$, $k_G=1.13$ $Pa.m$)
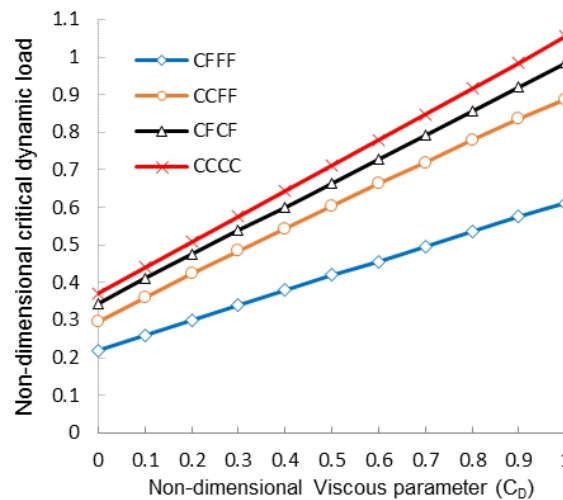

Fig. 8. Viscous damper in viscoelastic foundation versus various boundary conditions ($\Omega=2$, $e_0a=2nm$, $k1=1$; $k2=0$, $\beta=1$, $k_G=1.13$ $Pa.m$, $k_w=1.13GPa/nm$).

Fig. 9 displays the nanoscale factor versus a dimensionless ratio (h/L_x). To this aim, both longitudinal and lateral dimensions of the plate are the same and fixed, and its thickness can be changed. Two cases for loading versus two boundary conditions were considered. As the thickness increases, the impact of the nanoscale factor on the outcomes increase as well. As shown, due to the striking difference between the studied cases, as the boundaries are less flexible, the effect of the load type (uniaxial or biaxial) on the boundary conditions will dramatically increase. All in all, it should be stated that the thickness has a significant effect on both value and kind of dynamic loads.

To consider the difference percent between the dynamic and static buckling, Eq. (29) is defined as follows:

$$Different\ percent\left(DP\right)=\left|\frac{Dynamic\ buckling\ load_{\sigma\neq0}-Static\ buckling\ load_{\sigma=0}}{Static\ buckling\ load_{\sigma=0}}\right|\times100 \qquad (29)$$
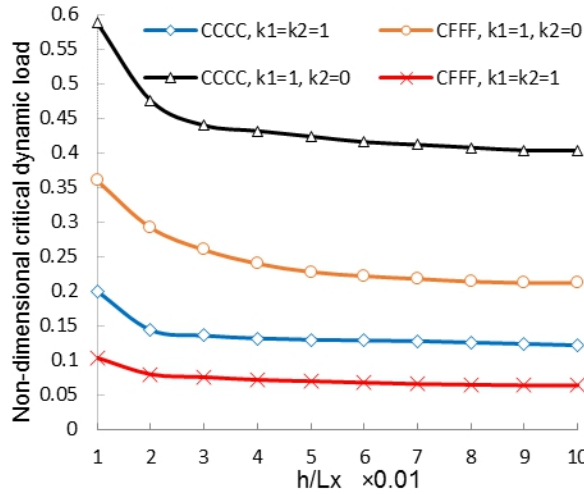
Fig. 9. Thickness to length ratio's influence on the critical dynamic load ($\Omega=2$, $C_D=0.1$, $k1=1$; $k2=0$, $\beta=1$)

The defined *DP* versus the nanoscale factor and the aspect ratio are plotted in Figs. 10 (a) and (b). As shown in Fig. 10 (a), the difference percent of results after $\mu=3nm^2$ is dramatically increased. In fact, before adding the above-mentioned value, the small scale effect has not shown noticeable effect on the outcomes of dynamic buckling loads versus static ones which means that for the larger nanoscale factor, the difference percent is quite important.

Fig. 10 (b) shows the results for which greater aspect ratio leads to a reduction in *DP*. It should be remarked that the difference percent for greater aspect ratio is much less than the lower one. On the whole, it is obvious that the length of the plate has a considerable effect on the critical dynamic loads of Gs.
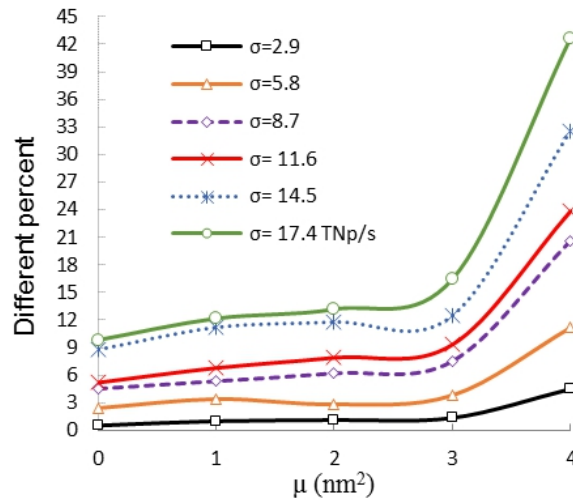

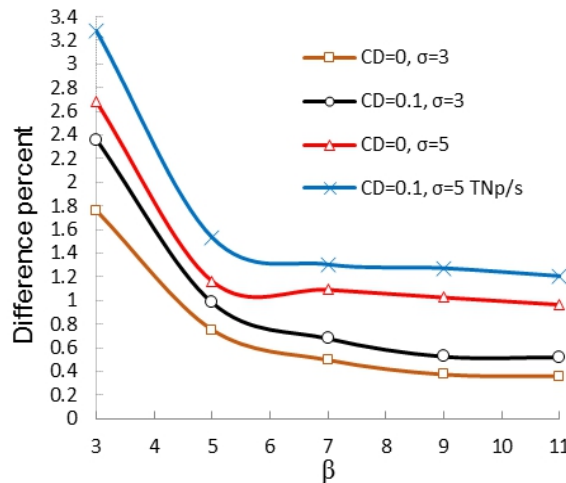**Fig. 10 (a).** The influences of the nanoscale factor on the difference percent (*CFCF*, $C_D=0.2$, $k1=0$; $k2=1$, $Lx/Ly=1$).

Fig. 10 (b). The impact of β on the difference percent (*CCCC*, $e_0a=2nm$, $k1=1$; $k2=0$, $\beta=1$, $k_w=1.13GPa/nm$, $k_G=1.13\ Pa.m$)

6. Conclusion

In the present study, the dynamic stability of a nanoplate embedded in a viscoelastic medium was assessed. The constitutive equations were formulated using FSDT and were analyzed based on the non-local continuum theory of Eringen to examine the nano size effects. DQM helped us to conjunct several boundary conditions with stability equations and meet valuable outcomes. It is noteworthy that all the results of this study were obtained for the first mode of buckling. The following remarks are presented as valuable outcomes of the present research:

- As the growing ratio increases, the effect of the aspect ratio will show a considerable growth as well.
- Regarding the load direction effects, there is a major difference in non-local outcomes in contrast to local ones.
- As the Winkler parameter increase and boundaries show less flexibility, more influences on the dynamic loads are observed.
- For larger values of the nanoscale factor, the small scale has a noticeable impact on the dynamic buckling results versus static ones.
- For greater aspect ratios, the difference percent outcomes are relatively close to each other.

References

[1] Shijie, C., Hong, H., Hee Kiat, Ch., Numerical analysis of dynamic buckling of rectangular plates subjected to intermediate-velocity impact, *International Journal of Impact Engineering*, 25(2), 2001, 147-167.

[2] Hosseini-Ara, R., Mirdamadi, H.R., Khademyzadeh, H., Salimi, H., Thermal effect on dynamic stability of single-walled Carbon Nanotubes in low and high temperatures based on Nonlocal shell theory, *Advanced Materials Research*, 622-623, 2013, 959-964.

[3] Haftchenari, H., Darvizeh, M., Darvizeh, A., Ansari, R., Sharma, C.B., Dynamic analysis of composite cylindrical shells using differential quadrature method (DQM), *Composite Structures*, 78(2), 2007, 292–298.

[4] Tamura, Y.S., Babcock, C.D., Dynamic stability of cylindrical shells under step loading, *Journal of Applied Mechanics*, 42(1), 1975, 190-194

[5] Jabareen, M., Sheinman, I., Dynamic buckling of a beam on a nonlinear elastic foundation under step loading, *Journal of Mechanics of Materials and Structures*, 4, 2009, 7-8.

[6] Ramezannezhad Azarboni, H., Darvizeh, M., Darvizeh, A., Ansari, R., Nonlinear dynamic buckling of imperfect rectangular plates with different boundary conditions subjected to various pulse functions using the Galerkin method, *Thin-Walled Structures*, 94, 2015, 577–584.

[7] Wang, X., Yang, W.D., Yang, S., Dynamic stability of carbon nanotubes reinforced composites, *Applied Mathematical Modelling*, 38(11-12), 2014, 2934-2945.

[8] Petry, D., Fahlbusch, G, Dynamic buckling of thin isotropic plates subjected to in-plane impact, *Thin-Walled Structures*, 38(3), 2000, 267–283.

[9] Kubiak, T., Criteria of dynamic buckling estimation of thin-walled structures, *Thin-Walled Structures*, 45(10-11), 2007, 888–892.

[10] Reddy, J.N., Srinivasa, A.R., Non-linear theories of beams and plates accounting for moderate rotations and material length scales, *International Journal of Non-Linear Mechanics*, 66, 2014, 43-53.

[11] Ghorbanpour Arani, A., Shiravand, A., Rahi, M., Kolahchi, R., Nonlocal vibration of coupled DLGS systems embedded on Visco-Pasternak foundation, *Physica B*, 407, 2012, 4123–4131.

[12] Eringen, A.C., *Nonlocal Continuum Field Theories*, Springer-Verlag, New York, 2002.

[13] Eringen, A.C., Linear theory of non-local elasticity and dispersion of plane waves, *International Journal of Engineering Science*, 10(5), 1972, 425-435.

[14] Duan, W.H., Wang, C.M., Zhang, Y.Y., Calibration of nonlocal scaling effect parameter for free vibration of carbon nanotubes by molecular dynamics, *Journal of Applied Physics*, 101(2), 2007, 24305-24311.

[15] Duan, W.H., Wang, C.M., Exact solutions for axisymmetric bending of micro/nanoscale circular plates based on nonlocal plate theory, *Nanotechnology*, 18(38), 2007, 385704.

[16] https://www.slideshare.net/zead28/concept-ofcomplexfrequency.

[17] Franco, S., *Electric Circuits Fundamentals*, Oxford University Press, Inc., 1995.

[18] Bellman, R., Kashef, B.G., Casti, J., Differential Quadrature: A Technique for the Rapid Solution of Nonlinear Partial Differential Equation, *Journal of Computational Physics*, 10(1), 1972, 40–52.

[19] Shu, C., *Differential Quadrature and Its Application in Engineering*, Springer, Berlin, 2000.

[20] Bellman, R., Casti, J., Differential quadrature and long-term integration, *Journal of Mathematical Analysis and Applications*, 34(2), 1971, 235–238.

[21] Chen, W., *Differential Quadrature Method and its Applications in Engineering*, Shanghai Jiao Tong University, 1996.

[22] Golmakani, M.E., Rezatalab, J., Non uniform biaxial buckling of orthotropic Nanoplates embedded in an elastic medium based on nonlocal Mindlin plate theory, *Composite Structures*, 119, 2015, 238-250.

[23] Murmu, T., Pradhan, S.C., Buckling analysis of a single-walled carbon nanotubes embedded in an elastic medium based on nonlocal elasticity and Timoshenko beam theory and using DQM, *Physica E*, 41(7), 2009, 1232–9.

[24] Golmakani, M.E., Sadraee Far, M.N., Buckling analysis of biaxially compressed double-layered graphene sheets with various boundary conditions based on nonlocal elasticity theory, *Microsystem Technologies*, 23(6), 2017, 2145-2161.

[25] Ansari, R., Sahmani, S., Prediction of biaxial buckling behavior of single-layered graphene sheets based on nonlocal plate

models and molecular dynamics simulations, *Applied Mathematical Modelling*, 37(12-13), 2013, 7338–7351.

[26] Malikan, M., Jabbarzadeh, M., Sh. Dastjerdi, Non-linear Static stability of bi-layer carbon nanosheets resting on an elastic matrix under various types of in-plane shearing loads in thermo-elasticity using nonlocal continuum, *Microsystem Technologies*, 23(7), 2017, 2973-2991.

[27] Malikan, M., Electro-mechanical shear buckling of piezoelectric nanoplate using modified couple stress theory based on simplified first order shear deformation theory, *Applied Mathematical Modelling*, 48, 2017, 196–207.

[28] Malikan, M., Analytical predictions for the buckling of a nanoplate subjected to non-uniform compression based on the four-variable plate theory, *Journal of Applied and Computational Mechanics*, 3(3), 2017, 218–228.

[29] Malikan, M., Buckling analysis of micro sandwich plate with nano coating using modified couple stress theory, J*ournal of Applied and Computational Mechanics*, 4(1), 2018, 1-15.

[30] Civalek, Ö., Korkmaz, A., Demir, Ç., Discrete singular convolution approach for buckling analysis of rectangular Kirchhoff plates subjected to compressive loads on two-opposite edges, *Advances in Engineering Software*, 41(4), 2010, 557-560.

[31] Dastjerdi, S., Jabbarzadeh, M., Nonlinear bending analysis of bilayer orthotropic graphene sheets resting on Winkler–Pasternak elastic foundation based on non-local continuum mechanics, *Composites Part B: Engineering*, 87, 2016, 161-175.

[32] Karličić, D., Adhikari, S., Murmu, T., Cajić, M., Exact closed-form solution for non-local vibration and biaxial buckling of bonded multi- nanoplate system, *Composites Part B*, 66, 2014, 328-339.